

Ice plate deformation and cracking revealed by an in-situ distributed acoustic sensing array

Jun Xie¹, Xiangfang Zeng¹, Chao Liang², Sidao Ni¹, Risheng Chu¹, Feng Bao¹, Rongbing Lin¹, Benxin Chi¹, Hao Lv¹

5 ¹ State Key Laboratory of Geodesy and Earth's Dynamics, Innovation Academy for Precision Measurement Science and Technology, Chinese Academy of Sciences, Wuhan, 430077, China

² Institute for Disaster Management and Reconstruction (IDMR), Sichuan University, Chengdu, 610100, China

Correspondence to: Xiangfang Zeng (zengxf@whigg.ac.cn)

Abstract. Studying seismic sources and wave propagation in ice plates can provide valuable insights into understanding various processes such as ice structure dynamics, migration, fracture mechanics, mass balance, ~~and more etc.~~ However, the ~~extreme-harsh~~ environment ~~makes it difficult to conduct~~ ~~presents challenges that result in limited~~ in-situ dense seismic observations. Consequently, our understanding of the dynamic changes within the ice sheet remains insufficient. We conducted a seismic experiment using a distributed acoustic sensing (DAS) array on a frozen lake, exciting water vibrations through underwater airgun shots. By employing an artificial intelligence method, we were able to detect seismic ~~signals~~ ~~events~~ that includes both high frequency icequakes and low frequency events. The icequakes clustered along ice fractures and ~~its activity~~ correlated with local temperature variations. The waveforms of ~~low~~ frequency events exhibit characteristics of flexural-gravity waves which offers insights into the properties of ~~the~~ ice plate. Our study demonstrates the effectiveness of an ~~Distributed Acoustic Sensing~~ DAS array as an in-situ dense seismic network ~~in~~ for investigating the internal failure process and dynamic deformation of ice plates such as ice shelf, ~~which may~~ ~~-This research~~ contributes to an enhanced ~~comprehension and~~ prediction of ice shelf disintegrations.

1 Introduction

Cryo-seismology, ~~thanks due~~ to its high temporal resolution capabilities, has attracted the attention of scientists in the fields of seismology, cryosphere, and climatology. It ~~serves is regarded as as an~~ ~~valuable-effective tool-approach~~ for ~~investigating-studying~~ glacier dynamics and ~~comprehending-understanding complex~~ intricate processes (Aster and Winberry, 25 2017; Podolskiy and Walter, 2016). Seismological records of the cryosphere can be utilized to study the dynamic process occurring on the surface or within glaciers, ~~thereby-facilitating-aiding in~~ the identification of the ice shelf damage, ~~and~~ environmental changes ~~and so on-and other fields~~. Large glacial earthquakes can be detected by global seismic networks (~~for~~ ~~example-e.g.~~, Global Seismographic Network), and their mechanisms have been extensively studied, which ~~are-considered-to~~ ~~be-were~~ associated with iceberg calving and capsizing (Ekström et al., 2003; Sergeant et al., 2019; Veitch and Nettles, 2017). 30 ~~However-Besides~~, local microseismicities (such as surface crevasses and basal slip events) can provide more insights into the dynamic change process of glaciers and facilitate the study of glacier disintegration ~~in-a-mechanism~~ (Helmstetter et al., 2015;

Lombardi et al., 2019; Romeyn et al., 2021; Walter et al., 2013). Due to lower released seismic energy and stronger high attenuation for higher frequency signal excited by associated with these events, it is crucial to have closely spaced seismic stations (e.g., on the ice surface or in shallow boreholes) in order to accurately capture signal and analyse the data (Röösli et al., 2014; West et al., 2010). However, the complex-harsh environment and logistical challenges of glaciers make it difficult to deploy in-situ dense seismic array seismometers for comprehensive long term monitoring. As a result, researchers even explored the potential of utilizing a single seismometer to study icequakes (e.g., Köhler et al., 2019).

In recent years, ~~the use of~~ distributed acoustic sensing (DAS) arrays ~~has~~ been ~~tested-deployed~~ in glacier environments, ~~to study glacial structures and its with advantage~~ The benefits of their large aperture and dense observation ~~has~~ been ~~tested~~ ~~demonstreddemonstrated~~ ~~on glacier environment to in the~~ study ~~the of~~ glacial structures and the monitoring of detect its seismicities icequakes (Booth et al., 2020; Brisbourne et al., 2021; Castongia et al., 2017; Fichtner et al., 2022; Hudson et al., 2021; Walter et al., 2020). Hudson et al. (2021) conducted a study on using DAS to monitor basal icequakes at Rutford Ice Stream. ~~In their research, t~~They compared the performance of DAS with a geophone network-array in terms of microseism icequake detection and location. The study found the DAS is outperformed the geophone network-array in monitoring ~~the~~ microseism signals. Their methodology and findings are heuristic-useful for ~~the~~ applying of DAS in glacial environment. Walter et al. (2020) deployed a DAS network-array in Alpine terrain and they successfully detected glacier stick-slip events which are associated with glacier flow and nearby rock falls. Their work demonstrated the significant potential of DAS technology for seismic monitoring of glacier dynamics and natural hazards in the mountainous regions. These studies demonstrated logistical feasibility of installing a large aperture, high-quality DAS network-array in glacial environments. However, the deployment-use of DAS ~~on ice shelves for to~~ studying the interaction between water and ice on ice shelves has been limited.

In this study, we deployed a DAS network-array on the Xiliushui Reservoir, a frozen freshwater lake in Gansu Province, China to explore the effectiveness of using a-DAS array for monitoring the cracking and dynamic flexure of the ice plate (Fig. 1). Seismicities have been observed on frozen lakes similar to icequakes in ice shelf (e.g., Dobretsov et al., 2013; Kavanaugh et al., 2018; Ruzhich et al., 2009). Nziengui-Bâ et al. (2022) ~~measured-obtained~~ the thickness and Young's modulus of the ice pack of a lake with DAS ~~reerodsrecords of using~~ hammer testssignal. Fichtner et al. (2022) deployed fiber-optic cable on a frozen lake of a volcano and detected ~~the~~ volcanic tremors. In ~~our-this~~ study, we employed an underwater AirGun Excitation (AGE) to generate water waves and recorded the resulting water-ice plate vibrations. Using an AI-based method, we successively detected and classified various seismic events, including both icequakes and Low Frequency Events (LFEs). Subsequently, we conducted an analysis of the seismic signals, examining their waveform characteristics, event occurrence rates and locations. One of the key aspects of our analysis involved estimating the stiffness Young's modulus of the ice plate by studying the dispersion of flexural-gravity waves excited by LFEs. Finally, we discussed implications of our experiments for understanding the dynamics of ice shelves in natural settings.

2 Experimental setting

65 The experimental site for our study was the Zhangye airgun active source platform, located in Xiliushui Reservoir, ~~the~~
~~secondary reservoir of Zhangye Longshou Hydropower Station~~ in Qilian Mountain, Zhangye City, Gansu Province, China
(Fig. 1). The average elevation of the Zhangye airgun active source platform is approximately 1900 meters. The water depth
of the Xiliushui Reservoir ranges from 45 to 65 meters, and during the winter of Northern Hemisphere, the ice thickness in
70 the reservoir reaches around 0.5 meters. The active airgun source used in this study was positioned at the centre of the lake,
submerged at a depth of 15 meters beneath the water surface (Wei et al., 2018). It has been observed that the bubbles
generated by the airgun can induce water body vibration ~~(s, as described in the study by de Graaf et al., (2014). This makes~~
~~the airgun an effective source for simulating ocean waves.~~ The generated water body vibrations closely ~~resemble-mimic~~
the characteristics of natural ocean waves, ~~allowing-enabling for~~ realistic and controlled experiments in the study of ice and
wave interaction and related phenomena.

75 In our experiment, a 1.2 km long standard single-mode fiber-optic cable was installed on the surface of the ice ~~during~~
~~the period of January 6th to January 9th, 2020. To ensure proper coupling between the fiber-optic cable and the ice surface,~~
~~we poured water over the fiber-optic cable which, when frozen, formed a solid bond with the ice and effectively coupled the~~
~~fiber-optic cable to the ice surface.~~ The fiber-optic cable was laid in two circular patterns around the airgun floating platform.
The inner circle is about 340 meters long, spanning channels 470 to 645, and the outer circle is nearly 800 meters long,
80 encompassing channels 51-457 (Fig. 1). ~~To ensure proper coupling between the fiber optic cable and the ice surface, we~~
~~poured water over the fiber-optic cable. As the water froze, it formed a solid bond with the ice, effectively coupling the fiber-~~
~~optic cable to the ice surface.~~ The interrogator is an Ovlink DAS unit, ~~which calculates-measured longitudinal dynamic strain~~
~~rates recorded by the~~ ~~aof the nd the cable is a standard single-mode~~ fiber-optic cable. In this experiment, we employed a
gauge length of 2 meters, which refers to the length of the section of the fiber-optic cable used for measurements. The spatial
85 sampling interval was set at 2 meters, and the temporal sampling rate was set at 1000 Hz. The experiment ~~commenced~~
~~started~~ at 21:00 p.m. on January 6th (Beijing time) and ~~concluded-finished~~ at 17:00 p.m. on January 9th. Unfortunately, some
instrument failures occurred during the afternoon of January 8th, resulting in an incomplete record between 11:00 p.m. and
13:00 p.m. During the entire duration of the experiment, a total of 65 hours of data, amounting to nearly 600 GB was
90 recorded. Additionally, a CMG-40T three-component short-period seismometer, equipped with a RefTek 130B data logger,
was positioned on the shore to capture ground motion. This seismometer recorded data at a sampling rate of 50 Hz,
providing complementary information to the DAS recordings ~~obtained from the fiber-optic cable setup on the ice surface.~~

3 Seismic events

Throughout the experiment, a total of 239 AGEs were conducted. However, due to an instrumental issue, only 223
~~complete~~-AGEs were successively recorded. Previous studies indicated that the near-field AGE waveform mainly comprises
95 two components: the main pulse and low-frequency bubble signal ~~(de Graaf et al., 2014)~~. However, our observations with

DAS revealed that the near-field AGE signal exhibits a distinct main pulse (Fig. S1 in the supporting information). Additionally, we observed that the similarity ~~between~~ among different AGE waveforms was below 20% (Fig. S2 in the supporting information). The main reason for this phenomenon is likely ~~to~~-related to the short observation distance between the DAS array and the airgun source. This proximity may have caused the signal recorded by DAS to be clipped, resulting in the absence of a recognizable main pulse.

In addition to the AGE experiments, we also conducted ten hammering experiments to measure the velocity of seismic waves propagating in the ice plate. The hammering signal primarily contained energy above 100 Hz (Fig. S1 in the supporting information). In the hammering signal, a relatively weak P₋-wave signal can be observed. By ~~analysing~~ analyzing the DAS record along a line aligned with the hammering point, we estimated the P₋-wave velocity in the ice plate to be approximately 3,200 m/s (Fig. S3 in the supporting information). This estimation is consistent with previous research findings. For instance, ~~study conducted by~~ Ewing et al. (1934) indicated that ~~thick solid ice typically exhibits the~~ P-wave velocity in thick solid ice ranging ~~from between~~ from 3,432 ~~and to~~ 3,698 m/s. Similarly, Wen et al. (1991) reported that the P-wave velocity in thinner ice layers ~~are expected to have velocities ranging ranges~~ from 2,000 to 3,040 m/s.

Apart from the AGE and hammering signals, our observations revealed two types of passive source signals (Fig. 2). The first type corresponds to icequakes that occur within the ice plate and are characterized by a dominant energy at high frequencies ranging from over 10 Hz to ~~a few hundred~~ 100s Hz (Fig. 2). These signals are associated with longitudinal waves propagating through the ice plate that cause elongation along the fibre direction (Moreau et al., 2020). During the occurrence of some icequakes, the staff also reported hearing cracking sounds, which aligns previous observations reported by Kavanaugh et al. (2018). ~~This acoustic evidence provides further confirmation of the dynamic activity within the ice plate during seismic events.~~ The other type is characterized by energy primarily in the lower frequency range (1-10 Hz) and has a duration of ~~about pproximately~~ 1 second (Fig. 2). Considering its lower frequency signal, ~~w~~We termed them as Low Frequency Event (LFE). They typically emerged after AGEs and exhibit remarkably similar waveforms and moveouts as ~~depicted shown~~ in Fig. S4 in the supporting information.

4 Detection and location

The application of machine learning in seismology has experienced a significant growth in recent years. Machine learning techniques have been primarily focused on earthquake detection and phase-picking ~~methods~~, often applied to regional and global earthquake datasets that rely on conventional seismic ~~networks arrays~~ (Zhu and Beroza, 2019; Zhou et al., 2019; ~~Stork et al., 2020~~; Ross et al., 2018). In this study, we applied a convolutional neural network (CNN) known as You Only ~~LookSee~~ Once (YOLO, version 5) (Redmon and Farhadi, 2018) to efficiently scan ~~efficiently~~ through the DAS dataset ~~to detect the~~ for seismic events and ~~categorize~~ classify them into three ~~categories~~ groups: AGE, LFE and icequake. This CNN is designed for accurate real-time object detection in video files (Redmon and Farhadi, 2018) and has been successfully utilized for micro-seismic event detection in DAS records (Stork et al., 2020). We converted the record sections of DAS

~~waveforms-dataset~~ to images. To enhance the signal-noise-ratio (SNR), the DAS data is bandpass filtered within the range of 5-50 Hz and normalized based on the maximum amplitude of the entire record section. We assembled ~~6-second~~ of data from all channels (51-645) into an image, ensuring a 50% overlap to prevent misdetection. We then down sampled the image into a size of 600 by 600 pixels, resulting in each image being approximately 980 KB in size.

To train the AI model, we manually inspected the seismic data from the first 12 hours and ~~labelled~~ 60 AGEs, 122 LFEs and 360 icequakes. This ~~labeled~~-dataset was then ~~divided-split~~ this into training, validation, and test sets using a 4:1:1 ratio. ~~Since the AGE catalogue of AGEs was well-established, it was-and~~ used to evaluate the performance of the ~~trained~~ model. To accelerate the training process, we utilized a GPU, which reduced the training time to approximately 3 hours. The performance of the model on the test set is depicted in Fig. S5. The confusion rate was found to be low, indicating accurate classification results. For instance, no AGEs were misclassified as icequake. ~~The recall rate is calculated by dividing the number of True Positives (TP) by the total number of actual positives. TP represents the correct prediction, such as detecting icequake as icequake. The recall rate is the number of True Detectives (TP) divided by everything predicted as positive. TP is the True Prediction, that is, for example the icequake being detected as icequake.~~ The recall rates for AGEs, LFEs and icequakes are 100.0%, 100.0% and 91.0%, respectively, while the precision for the three ~~groups~~ are 73.0%, 93.0% and 62.8%, respectively. ~~This level of p~~~~The precision is is comparable to the results reported by Stork et al. (2020), indicating statistically meaningful characteristics of the study area.~~ Finally, we applied trained AI model to scan through the rest of the ~~seismic-dataset~~ (39,280 images). In total, we detected 14,498 icequakes and 9,391 LFEs.

To gain deeper insights into the mechanism of the seismic sources, we located the identified icequakes and LFEs, respectively. Here, we utilized an absolute location method based on the neighbourhood algorithm (Sambridge, 1999) ~~for precise determination of the seismic source locations~~. We assumed that the propagation velocity of seismic waves in the ice sheet is isotropic, and set it as an inversion parameter. Since the ice plate is thin, we assume the focal depth to be zero. We used ~~a~~ ~~the~~ ~~'short-time-average through long-time-average trigger'~~ (STA/LTA) method (Stevenson, 1976) to pick arrivals. The short and long time-windows are set to 0.05 s and 0.25 s for icequakes, and 0.5 s and 2.5 s for LFEs, respectively. ~~During the location inversion, the travel-time misfit of each pick is normalized (weighted with) by the maximum amplitude of each waveform.~~ To assess the ~~location~~-error of our ~~location setting~~ ~~location method~~, we located those 10 hammering events ~~and compared with their ground truth locations~~. The results showed that the minimum, maximum and average location errors of hammering events are 5 m, 20 m, and 10.2 m, respectively (Fig. S6 in the supporting information). It is important to note that most of the location results exhibited a bias towards the north direction. This systematic deviation of the location results could be attributed to the systematic bias in the position of fiber-optic cable. Overall, the accuracy of the location in this study is acceptable.

We detected 14,498 icequakes, exhibiting a clear diurnal cycle (Fig. 2c) and primarily clustered along the promising fractures (Fig. 2d). The number of icequakes does not seem to be associated with AGEs but is rather correlated with the local temperature variation (Fig. 2c). This phenomenon has also been reported by ~~other previous~~ studies, for instance, Goto et al.

(1980) observed that there was a strong correlation between the occurrence of ~~high-icequake activity~~ and the temporal variation of temperature differences within the ice plate. This reveals the nature of icequakes in our experiments as brittle failure of ice plate caused by uneven thermal expansion. The icequake interevent distribution follows a Poisson distribution (Fig. S7 in the supporting information), suggesting that the occurrence of icequakes is random, similar to tectonic earthquakes (Rydelek and Sacks, 1989). This implies that there is no specific temporal or spatial pattern governing the occurrence of icequakes, and they occur independently of each other. ~~It provides valuable insights into the nature of icequake occurrence in the ice plate.~~ This information is important for understanding the behaviour of icequakes and ~~their-its~~ relationship to other geophysical phenomena. It is worth noting the surge of icequake activity since the noon of January 9th probably indicates a heightened development of cracks within the ice plate. There also seems to be a slight delay between the icequake activity and the temperature, which is probably due to lag from thermal diffusion. ~~A similar delay was reported in According to the study of~~ (Goto et al. (1980), ~~in which~~ the time lag is about 2 hours. In ~~our-this~~ study, we did not directly measure the ice temperature, but instead relied on the air temperature data. Future work should consider incorporating a combined approach using distributed temperature sensing (DTS) (e.g., Selker et al., 2006) as well as in-situ DAS observations to establish a more accurate correlation between temperature variations and ~~seismic-icequake~~ activity. Besides, ~~to gain a more comprehensive understanding of the relationship requires~~ a longer observation period in real glacial environments ~~is required to gain a more comprehensive understanding of the relationship requires~~.

~~Among all the detected events, a total of 9,391 were classified as LFEs. Out of the total number of detected events, 9,391 LFEs were observed.~~ These LFEs exhibit a tendency to cluster primarily in the central region of the lake, as well as in close proximity to the airgun floating platform (Fig. 2d). The analysis reveals a close association between LFEs and AGEs, with LFEs generally following AGEs closely in time. However, the detectability of LFEs may vary for different AGEs due to varying noise levels. ~~It is observed that~~ LFEs ~~are predominantly detected within the first 5 minutes following become AGE, but become more~~ challenging to observe ~~approximately 5 minutes after the occurrence of AGEs thereafter~~ (Fig. 2c and further supported by Fig. S8 in the supporting information). In the meantime, the ~~interevent~~ occurrence ~~interval~~ of LFEs does not follow ~~a-the~~ Poisson distribution (Fig. S9 in the supporting information). These observations suggest that there may be a temporal relationship or dependency between AGEs and LFEs, indicating potential interactions or triggering mechanisms between these seismic events and LFEs are likely the water~~body~~ vibrations following the AGEs.

5 Dispersion curve of LFE

Extracting the dispersion relation from the waveforms of LFEs is a valuable approach to ~~gaining a~~ deeper understanding of ~~their physical-LFE~~ mechanism and ~~signal signal~~ propagation. ~~Since the LFEs waveforms share a similar moveout patterns (Fig. S4 in the supporting information), In order to enhance the signal-to-noise ratio (SNR) of the LFEs, we stacked similar waveforms from a series of LFEs to improve SNR employed a technique of waveform stacking. This is applicable because the LFEs waveforms share a similar moveout patterns (Fig. S4 in the supporting information).~~ By selecting a master LFE

event, we aligned the waveforms of other LFEs with by measuring the time shifts obtained from throughmoving cross-correlation analysis. ~~This stacking aligned waveforms process involves adding up the aligned waveforms, which effectively~~ increases the amplitude of the coherent LFE signals while ~~the random noise is reduced~~ reducing the contribution of random noise. ~~As a result, the stacked waveform provides a clearer and more distinct representation of the LFE activity, allowing for better analysis and interpretation of the underlying physical mechanisms~~ As a quality control, we applied a threshold for the cross-correlation coefficient to retain only the waveforms that ~~exhibited a strong correlation~~ well correlated with the master ~~LFE event waveform~~. Specifically, we considered waveforms with a cross-correlation coefficient greater than 0.7 as indicative of a significant correlation. ~~This criterion ensured that only high quality waveforms were included in the stacking process~~. The resulting stacked waveforms, which are shown in Fig. 3, exhibit a clear inverse dispersion pattern. This pattern implies that the LFE signals with higher frequencies arrive earlier than those with lower frequencies.

After obtaining the stacked LFE waveforms, we applied the multi-channel surface wave analysis method developed by Park et al. (1999) to extract the phase velocity dispersion curve. This method allows us to analyse the surface wave signals present in the stacked LFE waveforms and determine the variation of phase velocity with respect to frequency. In the frequency range of 1 to 15 Hz, the phase velocity of the LFEs varies from 20 to 160 m/s. This range of velocities is significantly lower than the typical shear wave velocity of ice, which is around 1400 m/s as reported by Hudson et al. (2021). This dispersion curve displays the distinctive characteristic of the Flexural-Gravity Wave (FGW) (Williams and Robinson, 1981), which is a special guided wave driven by restoring forces from ice plate flexure and gravity. It corresponds to the Quasi-Scholte mode (QS) seismic wavefield of a thin floating ice plate (Moreau et al., 2020; Nziengui-Bâ et al., 2022).

The phase velocity dispersion curve relation (relation of frequency (f) and wavenumber (k)) of FGW can be written as (Liu and Mollo-Christensen, 1988),

$$(2\pi f)^2 = \frac{(gk + Dk^5 - Qk^3)}{\coth kH + kM} \quad (1).$$

where g is the gravity acceleration, k is wavenumber, H is the water depth which is 60 meters in this study, D is the bending modulus, which is a function of ice properties, $D = Eh^3/\rho_w 12(1 - \nu^2)$, where E is the Young's modulus, ν is the Poisson ratio, h is the ice thickness which is 0.5 meters in this study, ρ_w is the density of water. Q is due to compression forces ice compression, $Q = Ph/\rho_i$, where ρ_i is the density of ice. M is due to the added mass of the ice sheet mass loading, $M = h\rho_i/\rho_w$. M and Q are much smaller than gravity and flexural terms and can be neglected (Sutherland and Rabault, 2016). The dispersion equation can be rewritten as,

$$(2\pi f)^2 = \frac{(gk + k^5 Eh^3/\rho_w 12(1 - \nu^2))}{\coth kH + kM} \quad (2).$$

The Young's Modulus can also be determined with compressional wave velocity V_p , $E = V_p^2 \rho (1 - \nu^2)$, assuming $\nu = 0.33$, according to the results from Fig. S3, E is 9.12 GPa.

The dispersion of the FGW is largely controlled by the ice plate thickness and ~~stiffness-Young's modulus~~ (Zhao et al., 2018; Sergienko, 2017; Sutherland & Rabault, 2016; Timco & Frederking, 1983; Yang & Yates, 1995). Given a roughly known ice plate thickness (~0.5 m), we successfully explained the observed dispersion curve using the theoretical prediction of FGW (equation 1) with an ice Young's modulus (E) around 10 GPa, ~~which- is very close to the one for fresh water ice (Timco & Weeks, 2010). However, Young's modulus and ice thickness are strongly correlated. Thus, a large uncertainty on one of the two parameters will have the same effect on the other. Therefore a joint inversion method combines quasi-Scholte mode and quasi-symmetric mode (corresponds to compressional waves) following a Bayesian scheme should be used to simultaneously invert the, both-~~ thickness and the Young's modulus, ~~and can obtain more accurate results (Nziengui-Bâ et al., 2022).~~ ~~In this case, the Young's modulus is 9.1 ± 0.2 GPa, and the thickness is 48 ± 0.1 cm, respectively.~~ ~~Since the frequency-thickness is much less than $50 \text{ Hz} \cdot \text{m}$, -we adopted the thin plate model (equation 1) is still valid in this study. In other case with thick ice plate, full elastic model (e.g., (Mindlin, 1951)-Mindlin, 1951) could be used-~~

6 Discussion

Indeed, ~~t~~the effective modulus of ice ~~is a measure of~~ reflects its elastic and viscous deformation characteristics, which can be influenced by various factors, including strain rate, temperature, density, ice type, purity and existence of cracks, etc. (Sinha, 1989). Considering the complex nature of ice and its sensitivity to various factors, understanding the effective modulus provides valuable insights into the deformation behaviour and mechanical properties of ice under different conditions. Researchers study these relationships to improve our understanding of ice mechanics and its applications in various fields, such as glaciology, geophysics, and engineering. In the study of Nziengui-Bâ et al. (2022), the Young's Modulus ~~are-is~~ below 5 GPa. They suspected that ~~this~~ value ~~of E~~ is underestimated due to snow layer covering the ice surface or ~~heterogeneity/inhomogeneity~~/porosity of the solid columnar ice layer. ~~In this study, the lake surface is covered with clear ice free from snow, implying a stronger stiffness.~~ In the study by Gold (1988), the Young's modulus ~~of the ice plate was found to be within~~ falls into the range of 4.7-10.4 GPa. ~~This range represents the stiffness or rigidity of the ice material, with higher values indicating greater stiffness.~~ Northwood (1947) ~~conducted an inversion analysis and~~ estimated the Young's modulus of ice to be 9.8 GPa. This value falls within the range reported by Gold (1988) and provides additional support for the ~~stiffness-Young's Modulus~~ of ice. Another study by Petrovic (2003) reported a slightly wider range for the Young's modulus of ice, between 9.7 and 11.2 GPa. ~~This range encompasses the values reported by both Gold (1988) and Northwood (1947), indicating consistency in the estimation of ice stiffness.~~

Deformations caused by ocean waves, such as FGW, play a significant role in the stability of ice shelves and can potentially result in their fragmentation or trigger calving events (Collins III et al., 2015; Liu and Mollo-Christensen, 1988). ~~H~~however, ~~previous studies have had limited~~ direct observations of the dispersion of the FGW ~~is limited in previous studies (e.g., Sutherland and Rabault, 2016).~~ In this ~~work~~study, we successfully obtained clear recordings of the FGW ~~using DAS.~~ ~~Actually, t~~The dispersion of FGW ~~is more sensitive to the ice plate thickness~~ can be used to estimate thickness of the ice

255 ~~plate, which is of significant importance, especially in situations where ice thickness determination is not well resolved, as~~
~~commonly encountered on ice shelves, this approach holds significant value, particularly in cases where the determination of~~
~~ice thickness is not well resolved, as commonly encountered on ice shelves.~~ Therefore, the accurate recording of FGW on
DAS provides a valuable means for inferring both the ice shelf thickness and ~~stiffness~~ Young's Modulus. In ~~the case of a~~
260 ~~cracked ice plates,~~ it is commonly observed that the ~~stiffness-strength~~ usually decreases compared to ~~the elastic modulus of~~
the individual grains, which is typically ~~measures~~ around 12 GPa. This suggests that the thickness of the grain boundaries
could potentially be estimated using the effective modulus ~~value~~ (Wang et al., 2008) ~~Wang et al., 2008~~. ~~For example,~~
~~(Renshaw et al., (2020), also reported found that the Young's modulus initially is around 9.5 GPa but starts to decrease once~~
~~the ice is compressed uniaxially and saturates at about 8.5 GPa along the loading direction and 7 GPa along two other~~
~~directions perpendicular to the loading direction.~~ In our studycase, the presence of the AGE resulted in severe fracturing of
265 the ice plate near the AirGun floating platform (Fig. 1). The dispersion curves of FGW for inner circle corroborate our
speculation (Fig. S10 in the supporting information), which also provide an explanation for the observed lower
velocity of FGW around 10 Hz in Fig. 3c. The dispersion curve of FGW obtained from the hammer signal (red triangle in
Fig. 1) also reveals a smaller Young's modulus (Fig. S11 in the supporting information). While our experiment was
conducted over a 3-day period on a frozen lake spanning a few hundred meters, we acknowledged its limitations in terms of
270 duration and spatial coverage. However, ~~with longer continuous observation periods of LFEs,~~ it ~~becomes-is~~ possible to
monitor the temporal variations in ~~stiffness-Young's Modulus~~ or thickness of the ice shelf plate with longer continuous
observations. Additionally, deploying a longer DAS cable holds the potential to capture the attenuation effect of the ice plate,
as highlighted by previous studies (e.g., Yang and Yates, 1995). This would not only enhance our understanding of wave
propagation characteristics but also provide valuable insights into the dynamic changes occurring within the ice plate and its
275 response to environmental changesfactors.

Previous studies have shown that FGW has the potential to induce icequakes on ice shelves. The interaction between
ocean waves and the ice shelf can lead to dynamic stress and strain variations, which can trigger seismic activities such as
icequakes. Studies such as Zhao et al. (2019) have shown that icequakes exhibit spatial and seasonal correlations with ocean
gravity waves. This association between icequakes and ocean waves suggests that the interaction between the two can have
280 significant implications for the stability and integrity of ice shelves (Zhao et al., 2019). The energy transferred from the
ocean waves to the ice shelf through processes like flexure and wave-induced vibrations can contribute to the fracturing and
weakening of the ice, ultimately increasing the risk of ice shelf disintegration. Olinger et al. (2019) found thermal and tidal
stresses are important in generating icequakes on the ice shelf. In our experiment, we observed that the number of icequakes
did not show a significant change after the AGE (Fig. S12 in the supporting information). This suggests that there may not
285 be a strong correlation between the airgun shot or FGW and the occurrence of icequakes. It is important to note that the
absence of a clear correlation in our experiment does not necessarily rule out the possibility of interactions between
icequakes and these external factors in other contexts or under different conditions. We even observed a slight decrease in
the number of icequakes after the AGE, which could be attributed to the reduced detection capability caused by strong AGE

coda. This discrepancy highlights the potential structural difference between the ice plate on a frozen lake and a real ice shelf.

290 It emphasizes the importance of conducting more on-site seismic observations on real ice shelves to gain a deeper understanding of their dynamics and behaviour. Future studies incorporating comprehensive field observations on actual ice shelves will provide valuable insights into the ~~seismic~~ response and behaviour of icequakes, leading to a better understanding of the factors influencing ~~their icequake~~ occurrence and the potential impacts on ice shelf stability. Moreover, DAS array on the seafloor is necessary to monitor the ocean wave and study the response of the ice shelf to the ocean waves ~~Moreover, DAS array on the seafloor is necessary to monitor the ocean wave and study the response of the ice shelf to the ocean waves~~ (Lindsey et al., 2019).

Our ~~research study~~ highlights the ~~considerable~~ potential of DAS in monitoring the formation and progression of ice cracks using passive source signals recorded in similar ice shelf studies. ~~This approach is~~, particularly ~~useful~~ in cases where there is a firm layer on the ice and remote sensing methods are challenging to employ. Furthermore, the variations of FGW can offer valuable information about the ~~inhomogeneity heterogeneity~~ of ice plate ~~stiffness Young's modulus~~, which can potentially help infer the size and distribution of the ice plate fragments. It is important to note that our experiment was conducted on an ice-covered lake, and to extend the applicability of these findings to ice shelves, spatial sampling and optimization of the array layout should be ~~essential~~ considered. For example, by deploying fiber-optic cable spanning hundreds of meters, we can accurately locate icequakes with a precision of meters, and we can also measure ~~longer wavelength~~ FGW ~~with a wavelength of dozens of meters~~. However, ~~measuring FGW induced by ocean wave on ice shelf becomes challenges, since longer wavelength (up to 10 s*-km) requires larger aperture array and dominant frequency is down to 0.1 Hz .when it comes to ice shelves with thickness reaching hundreds of meters and a length spanning tens of kilometres, measuring FGW induced by ocean waves presents unique challenges. In these cases, the wavelength of FGW can extend to several kilometres for periods longer than 10 seconds~~ (Zhao et al., 2018). By extending the length of the fiber-optic cable to several kilometres, we can probably capture FGW with larger wavelengths. However, there are other limitations that need to be addressed in future studies, for example, the coupling of fiber-optic cables with the ice on real ice shelves presents a significant challenge in practical applications due to harsh environmental conditions. Moreover, the conventional DAS fibre only measures a single strain component along the cable and does not provide polarization information, which increases the difficulty of identifying seismic phases (Hudson et al., 2021), and the absence of horizontal shear mode introduces additional uncertainty in estimating ice properties (Nziengui-Bâ et al., 2022). One potential remedy to address this is ~~to use~~ helically wound fibre (Ning and Sava, 2018).

7 Conclusion

In this study, we deployed a dense DAS ~~network array~~ on a frozen lake, ~~allowing us~~ to capture a wealth of near-field seismic signals generated by various phenomena occurring within the ice plate. Specifically, we focused on two types of seismic events: cracking, known as icequakes and dynamic flexure, referred as LFEs. We were able to obtain detailed and

comprehensive recordings of these seismic signals. The icequakes, which are associated with cracking and fracturing of the ice, were detected, and analysed to understand their characteristics and spatial distribution. Additionally, the LFEs, which result from the dynamic flexure of the ice plate, provide a tight constraint on the ice ~~stiffness~~ Young's modulus. This study has demonstrated the exceptional capability of the DAS array in accurately mapping the internal fractures and monitoring the strength of ice shelves. ~~By harnessing the unique sensing capabilities of DAS, we were able to capture detailed seismic signals associated with ice cracking and dynamic flexure, providing valuable insights into the behaviour of ice plates.~~ When combined with other remote sensing techniques, such as those employed by (Massom et al., 2018), DAS has the potential to greatly enhance our understanding and monitoring of ice shelf disintegration. The integration of DAS data with complementary remote sensing observations offers a comprehensive approach to studying ice shelf dynamics. This integrated approach provides a powerful tool for assessing the health and vulnerability of ice shelves, as well as tracking their responses to environmental factors and climate change.

Author contributions

XZ, ~~SN~~ planned the campaign; RL performed the measurements; JX, XZ, CL, FB and HL analysed the data; JX wrote the manuscript draft; JX, XZ, CL, SN, RC, BC and FB reviewed and edited the manuscript.

Code and data availability

The DAS event data is available on <https://www.zenodo.org/record/7424310>. YOLOv5 can be found <https://github.com/ultralytics/yolov5>. NA code can be found <http://rses.anu.edu.au/~malcolm/na/>

Competing interests

The authors declare that they have no conflict of interest.

Acknowledgements

The authors thank Baoshan Wang, Rui Zou, Yahong Wang for their help on the experiment setup and data requisition. We thank Herb Wang and Daoyuan Sun for their professional suggestions. The authors thank two anonymous reviewers and editors for their constructive comments.

Financial support

345 This work was supported by the National Natural Science Foundation of China with grant number 42274076, [42325401](#) and [42030311](#), the Youth Innovation Promotion Association of the Chinese Academy of Sciences under grant No. 2022335, and [and the Foundation for Innovative Research Groups of the Hubei Natural Science Foundation \(2023FA040\)](#).

References

- Aster, R. C. and Winberry, J. P.: Glacial seismology, *Rep. Prog. Phys.*, 80, 126801, <https://doi.org/10.1088/1361-6633/aa8473>, 2017.
- 350 Booth, A. D., Christoffersen, P., Schoonman, C., Clarke, A., Hubbard, B., Law, R., Doyle, S. H., Chudley, T. R., and Chalari, A.: Distributed Acoustic Sensing of Seismic Properties in a Borehole Drilled on a Fast-Flowing Greenlandic Outlet Glacier, *Geophysical Research Letters*, 47, e2020GL088148, <https://doi.org/10.1029/2020GL088148>, 2020.
- Brisbourne, A. M., Kendall, M., Kufner, S.-K., Hudson, T. S., and Smith, A. M.: Downhole distributed acoustic seismic profiling at Skytrain Ice Rise, West Antarctica, *The Cryosphere*, 15, 3443–3458, <https://doi.org/10.5194/tc-15-3443-2021>, 2021.
- 355 Castongia, E., Wang, H. F., Lord, N., Fratta, D., Mondanos, M., and Chalari, A.: An Experimental Investigation of Distributed Acoustic Sensing (DAS) on Lake Ice, *JEEG*, 22, 167–176, <https://doi.org/10.2113/JEEG22.2.167>, 2017.
- Chen, Z., Bromirski, P. D., Gerstoft, P., Stephen, R. A., Wiens, D. A., Aster, R. C., and Nyblade, A. A.: Ocean-excited plate waves in the Ross and Pine Island Glacier ice shelves, *Journal of Glaciology*, 64, 730–744, <https://doi.org/10.1017/jog.2018.66>, 2018.
- 360 Chen, Z., Bromirski, P. D., Gerstoft, P., Stephen, R. A., Lee, W. S., Yun, S., Olinger, S. D., Aster, R. C., Wiens, D. A., and Nyblade, A. A.: Ross Ice Shelf Icequakes Associated With Ocean Gravity Wave Activity, *Geophysical Research Letters*, 46, 8893–8902, <https://doi.org/10.1029/2019GL084123>, 2019.
- 365 Collins III, C. O., Rogers, W. E., Marchenko, A., and Babanin, A. V.: In situ measurements of an energetic wave event in the Arctic marginal ice zone, *Geophysical Research Letters*, 42, 1863–1870, <https://doi.org/10.1002/2015GL063063>, 2015.
- Dobretsov, N. L., Ruzhich, V. V., Psakhie, S. G., Chernykh, E. N., Shilko, E. V., Levina, E. A., and Ponomareva, E. I.: Advance in earthquake prediction by physical simulation on the baikal ice cover, *Phys Mesomech*, 16, 52–61, <https://doi.org/10.1134/S1029959913010062>, 2013.
- 370 Ekström, G., Nettles, M., and Abers, G. A.: Glacial Earthquakes, *Science*, 302, 622–624, <https://doi.org/10.1126/science.1088057>, 2003.
- Ewing, M., Crary, A. P., and Thorne, A. M., Jr.: Propagation of Elastic Waves in Ice. Part I, *Physics*, 5, 165–168, <https://doi.org/10.1063/1.1745245>, 2004.

- Fichtner, A., Klaasen, S., Thrastarson, S., Çubuk-Sabuncu, Y., Paitz, P., and Jónsdóttir, K.: Fiber-Optic Observation of
375 Volcanic Tremor through Floating Ice Sheet Resonance, *The Seismic Record*, 2, 148–155,
<https://doi.org/10.1785/0320220010>, 2022.
- Gold, L. W.: On the elasticity of ice plates, *Can. J. Civ. Eng.*, 15, 1080–1084, <https://doi.org/10.1139/l88-140>, 1988.
- Goto, K., H, H., and Y, W.: A study on ice faulting and icequake activity in the lake Suwa, (3) icequake activity and thermal stresses in ice plate, *The science reports of the Tohoku University. Fifth series, Tohoku Geophysical Journal*, 1980.
- 380 de Graaf, K. L., Brandner, P. A., and Penesis, I.: The pressure field generated by a seismic airgun, *Experimental Thermal and Fluid Science*, 55, 239–249, <https://doi.org/10.1016/j.expthermflusci.2014.02.025>, 2014.
- Helmstetter, A., Nicolas, B., Comon, P., and Gay, M.: Basal icequakes recorded beneath an Alpine glacier (Glacier d'Argentière, Mont Blanc, France): Evidence for stick-slip motion?, *Journal of Geophysical Research: Earth Surface*, 120, 379–401, <https://doi.org/10.1002/2014JF003288>, 2015.
- 385 Hudson, T. S., Baird, A. F., Kendall, J. M., Kufner, S. K., Brisbourne, A. M., Smith, A. M., Butcher, A., Chalari, A., and Clarke, A.: Distributed Acoustic Sensing (DAS) for Natural Microseismicity Studies: A Case Study From Antarctica, *Journal of Geophysical Research: Solid Earth*, 126, e2020JB021493, <https://doi.org/10.1029/2020JB021493>, 2021.
- Kavanaugh, J., Schultz, R., Andriashek, L. D., van der Baan, M., Ghofrani, H., Atkinson, G., and Utting, D. J.: A New Year's Day icebreaker: icequakes on lakes in Alberta, Canada, *Canadian Journal of Earth Sciences*, 56, 183–200,
390 <https://doi.org/10.1139/cjes-2018-0196>, 2018.
- Köhler, A., Maupin, V., Nuth, C., and Pelt, W. van: Characterization of seasonal glacial seismicity from a single-station on-ice record at Holtedahlfonna, Svalbard, *Annals of Glaciology*, 60, 23–36, <https://doi.org/10.1017/aog.2019.15>, 2019.
- Lindsey, N. J., Dawe, T. C., and Ajo-Franklin, J. B.: Illuminating seafloor faults and ocean dynamics with dark fiber distributed acoustic sensing, *Science*, 366, 1103–1107, <https://doi.org/10.1126/science.aay5881>, 2019.
- 395 Liu, A. K. and Mollo-Christensen, E.: Wave Propagation in a Solid Ice Pack, *Journal of Physical Oceanography*, 18, 1702–1712, [https://doi.org/10.1175/1520-0485\(1988\)018<1702:WPIASI>2.0.CO;2](https://doi.org/10.1175/1520-0485(1988)018<1702:WPIASI>2.0.CO;2), 1988.
- Lombardi, D., Gorodetskaya, I., Barruol, G., and Camelbeeck, T.: Thermally induced icequakes detected on blue ice areas of the East Antarctic ice sheet, *Annals of Glaciology*, 60, 45–56, <https://doi.org/10.1017/aog.2019.26>, 2019.
- Massom, R. A., Scambos, T. A., Bennetts, L. G., Reid, P., Squire, V. A., and Stammerjohn, S. E.: Antarctic ice shelf
400 disintegration triggered by sea ice loss and ocean swell, *Nature*, 558, 383–389, <https://doi.org/10.1038/s41586-018-0212-1>, 2018.
- Mindlin, R. D.: Influence of Rotatory Inertia and Shear on Flexural Motions of Isotropic, Elastic Plates, *Journal of Applied Mechanics*, 18, 31–38, <https://doi.org/10.1115/1.4010217>, 1951.
- Moreau, L., Boué, P., Serriperri, A., Weiss, J., Hollis, D., Pondaven, I., Vial, B., Garambois, S., Larose, É., Helmstetter, A.,
405 Stehly, L., Hillers, G., and Gilbert, O.: Sea Ice Thickness and Elastic Properties From the Analysis of Multimodal Guided Wave Propagation Measured With a Passive Seismic Array, *Journal of Geophysical Research: Oceans*, 125, e2019JC015709, <https://doi.org/10.1029/2019JC015709>, 2020.

- Ning, I. L. C. and Sava, P.: High-resolution multi-component distributed acoustic sensing, *Geophysical Prospecting*, 66, 1111–1122, <https://doi.org/10.1111/1365-2478.12634>, 2018.
- 410 Northwood, T. D.: Sonic determination of the elastic properties of ice, *Can. J. Res.*, 25a, 88–95, <https://doi.org/10.1139/cjr47a-011>, 1947.
- Nziengui-Bâ, D., Coutant, O., Moreau, L., and Boué, P.: Measuring the thickness and Young’s modulus of the ice pack with DAS, a test case on a frozen mountain lake, *Geophysical Journal International*, ggac504, <https://doi.org/10.1093/gji/ggac504>, 2022.
- 415 Olinger, S. D., Lipovsky, B. P., Wiens, D. A., Aster, R. C., Bromirski, P. D., Chen, Z., Gerstoft, P., Nyblade, A. A., and Stephen, R. A.: Tidal and Thermal Stresses Drive Seismicity Along a Major Ross Ice Shelf Rift, *Geophysical Research Letters*, 46, 6644–6652, <https://doi.org/10.1029/2019GL082842>, 2019.
- Park, C. B., Miller, R. D., and Xia, J.: Multimodal analysis of high frequency surface waves, in: *Proceedings of the symposium on the application of geophysics to engineering and environmental problems*, 00000, 115–121, 1999.
- 420 Petrovic, J. J.: Review Mechanical properties of ice and snow, *Journal of Materials Science*, 38, 1–6, <https://doi.org/10.1023/A:1021134128038>, 2003.
- Podolskiy, E. A. and Walter, F.: Cryoseismology, *Reviews of Geophysics*, 54, 708–758, <https://doi.org/10.1002/2016RG000526>, 2016.
- Redmon, J. and Farhadi, A.: YOLOv3: An incremental improvement, *ArXiv*, abs/184.02767, 2018.
- 425 Renshaw, C. E., Schulson, E. M., Iliescu, D., and Murzda, A.: Increased Fractured Rock Permeability After Percolation Despite Limited Crack Growth, *Journal of Geophysical Research: Solid Earth*, 125, e2019JB019240, <https://doi.org/10.1029/2019JB019240>, 2020.
- Romeyn, R., Hanssen, A., Ruud, B. O., Stemland, H. M., and Johansen, T. A.: Passive seismic recording of cryoseisms in Adventdalen, Svalbard, *The Cryosphere*, 15, 283–302, <https://doi.org/10.5194/tc-15-283-2021>, 2021.
- 430 Rössli, C., Walter, F., Husen, S., Andrews, L. C., Lüthi, M. P., Catania, G. A., and Kissling, E.: Sustained seismic tremors and icequakes detected in the ablation zone of the Greenland ice sheet, *Journal of Glaciology*, 60, 563–575, <https://doi.org/10.3189/2014JoG13J210>, 2014.
- Ross, Z. E., Meier, M.-A., and Hauksson, E.: P Wave Arrival Picking and First-Motion Polarity Determination With Deep Learning, *Journal of Geophysical Research: Solid Earth*, 123, 5120–5129, <https://doi.org/10.1029/2017JB015251>, 2018.
- 435 Ruzhich, V. V., Psakhie, S. G., Chernykh, E. N., Bornyakov, S. A., and Granin, N. G.: Deformation and seismic effects in the ice cover of Lake Baikal, *Russian Geology and Geophysics*, 50, 214–221, <https://doi.org/10.1016/j.rgg.2008.08.005>, 2009.
- Rydelek, P. A. and Sacks, I. S.: Testing the completeness of earthquake catalogues and the hypothesis of self-similarity, *Nature*, 337, 251–253, <https://doi.org/10.1038/337251a0>, 1989.
- 440 Sambridge, M.: Geophysical inversion with a neighbourhood algorithm—I. Searching a parameter space, *Geophysical Journal International*, 138, 479–494, <https://doi.org/10.1046/j.1365-246X.1999.00876.x>, 1999.

- Selker, J., van de Giesen, N., Westhoff, M., Luxemburg, W., and Parlange, M. B.: Fiber optics opens window on stream dynamics, *Geophysical Research Letters*, 33, <https://doi.org/10.1029/2006GL027979>, 2006.
- Sergeant, A., Mangeney, A., Yastrebov, V. A., Walter, F., Montagner, J.-P., Castelnau, O., Stutzmann, E., Bonnet, P.,
445 Ralaiarisoa, V. J.-L., Bevan, S., and Luckman, A.: Monitoring Greenland ice sheet buoyancy-driven calving discharge using glacial earthquakes, *Annals of Glaciology*, 60, 75–95, <https://doi.org/10.1017/aog.2019.7>, 2019.
- Sergienko, O. V.: Behavior of flexural gravity waves on ice shelves: Application to the Ross Ice Shelf, *Journal of Geophysical Research: Oceans*, 122, 6147–6164, <https://doi.org/10.1002/2017JC012947>, 2017.
- Sinha, N. K.: Elasticity of natural types of polycrystalline ice, *Cold Regions Science and Technology*, 17, 127–135,
450 [https://doi.org/10.1016/S0165-232X\(89\)80003-5](https://doi.org/10.1016/S0165-232X(89)80003-5), 1989.
- Stevenson, P. R.: Microearthquakes at Flathead Lake, Montana: A study using automatic earthquake processing, *The Bulletin of the Seismological Society of America*, 66, 61–80, <https://doi.org/10.1785/BSSA0660010061>, 1976.
- Stork, A. L., Baird, A. F., Horne, S. A., Naldrett, G., Lapins, S., Kendall, J.-M., Wookey, J., Verdon, J. P., Clarke, A., and
455 Williams, A.: Application of machine learning to microseismic event detection in distributed acoustic sensing data, *GEOPHYSICS*, 85, KS149–KS160, <https://doi.org/10.1190/geo2019-0774.1>, 2020.
- Sutherland, G. and Rabault, J.: Observations of wave dispersion and attenuation in landfast ice, *Journal of Geophysical Research: Oceans*, 121, 1984–1997, <https://doi.org/10.1002/2015JC011446>, 2016.
- Timco, G. W. and Frederking, R. M. W.: Flexural strength and fracture toughness of sea ice, *Cold Regions Science and Technology*, 8, 35–41, [https://doi.org/10.1016/0165-232X\(83\)90015-0](https://doi.org/10.1016/0165-232X(83)90015-0), 1983.
- 460 Veitch, S. A. and Nettles, M.: Assessment of glacial-earthquake source parameters, *Journal of Glaciology*, 63, 867–876, <https://doi.org/10.1017/jog.2017.52>, 2017.
- Walter, F., Dalban Canassy, P., Husen, S., and Clinton, J. F.: Deep icequakes: What happens at the base of Alpine glaciers?, *Journal of Geophysical Research: Earth Surface*, 118, 1720–1728, <https://doi.org/10.1002/jgrf.20124>, 2013.
- Walter, F., Gräff, D., Lindner, F., Paitz, P., Köpfli, M., Chmiel, M., and Fichtner, A.: Distributed acoustic sensing of
465 microseismic sources and wave propagation in glaciated terrain, *Nature Communications*, 11, 2436, <https://doi.org/10.1038/s41467-020-15824-6>, 2020.
- Wang, Y., Ballarini, R., and Rodin, G. J.: Crack-Tip Parameters in Polycrystalline Plates with Soft Grain Boundaries, *Journal of Engineering Mechanics*, 134, 100–109, [https://doi.org/10.1061/\(ASCE\)0733-9399\(2008\)134:1\(100\)](https://doi.org/10.1061/(ASCE)0733-9399(2008)134:1(100)), 2008.
- Wei, C., Qin, M., Zhang, Y., Zou, R., Wang, L., Guo, X., Liu, X., Wang, Y., and Sun, D.: Airgun Excitation Experiments at
470 Different Placement Depths in the Qilian Mountain of Gansu Province, China, *Seismological Research Letters*, 89, 974–982, <https://doi.org/10.1785/0220170253>, 2018.
- Wen, T., Garrison, G. R., Francois, R. E., Stein, R. P., and Felton, W. J.: Sound Speed, Reflectivity, and Absorption Measurements in Arctic Ice in 1988, sound speed reflectivity & absorption measurements in arctic ice in, 1991.
- West, M. E., Larsen, C. F., Truffer, M., O’Neel, S., and LeBlanc, L.: Glacier microseismicity, *Geology*, 38, 319–322,
475 <https://doi.org/10.1130/G30606.1>, 2010.

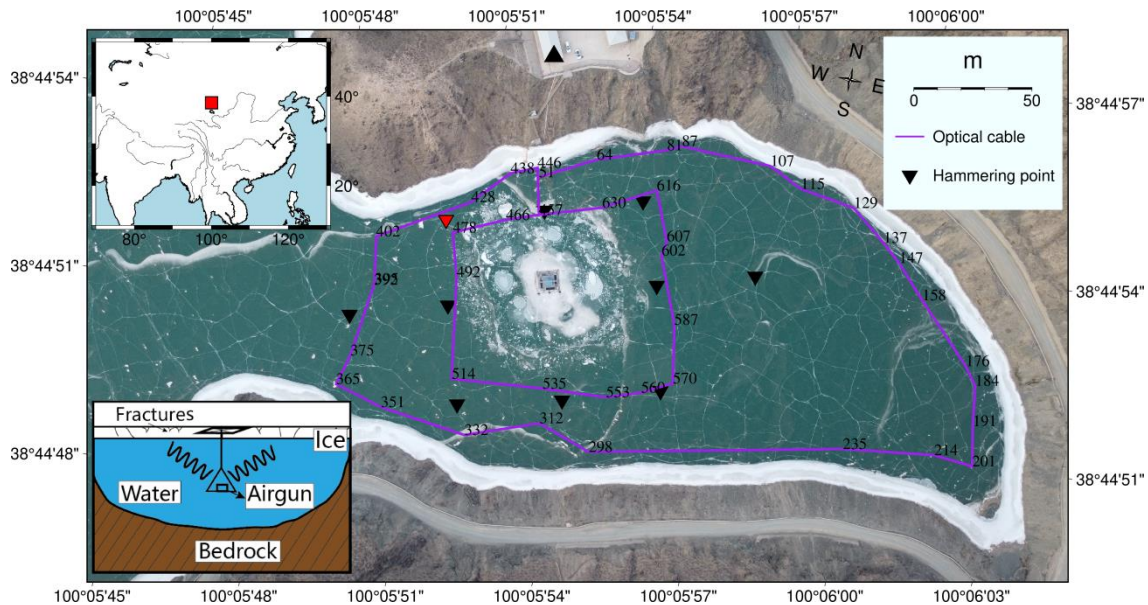
Williams, R. T. and Robinson, E. S.: Flexural waves in the Ross Ice Shelf, *Journal of Geophysical Research: Oceans*, 86, 6643–6648, <https://doi.org/10.1029/JC086iC07p06643>, 1981.

Yang, T. C. and Yates, T. W.: Flexural waves in a floating ice sheet: Modeling and comparison with data, *The Journal of the Acoustical Society of America*, 97, 971–977, <https://doi.org/10.1121/1.412076>, 1995.

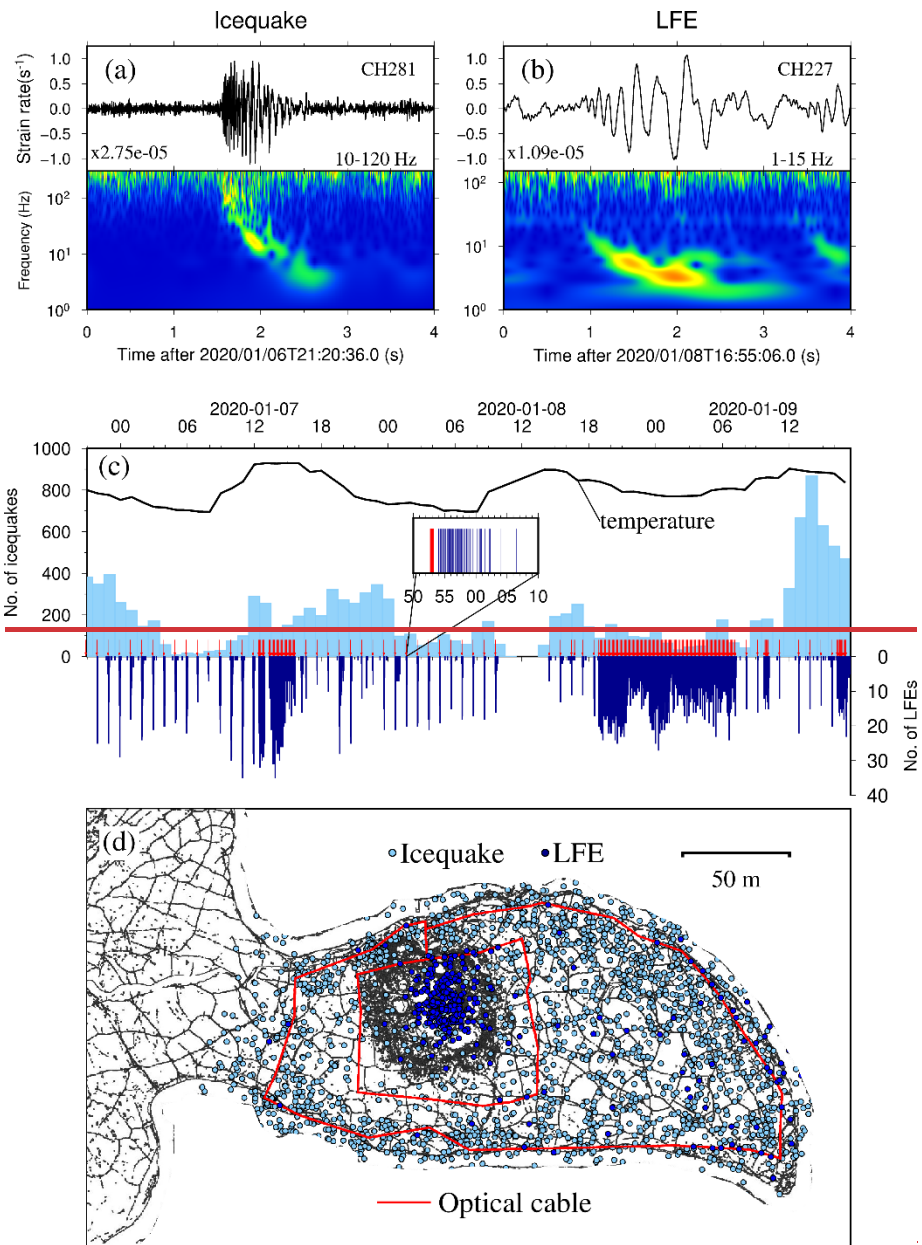
480 Zhou, Y., Yue, H., Kong, Q., and Zhou, S.: Hybrid Event Detection and Phase-Picking Algorithm Using Convolutional and Recurrent Neural Networks, *Seismological Research Letters*, 90, 1079–1087, <https://doi.org/10.1785/0220180319>, 2019.

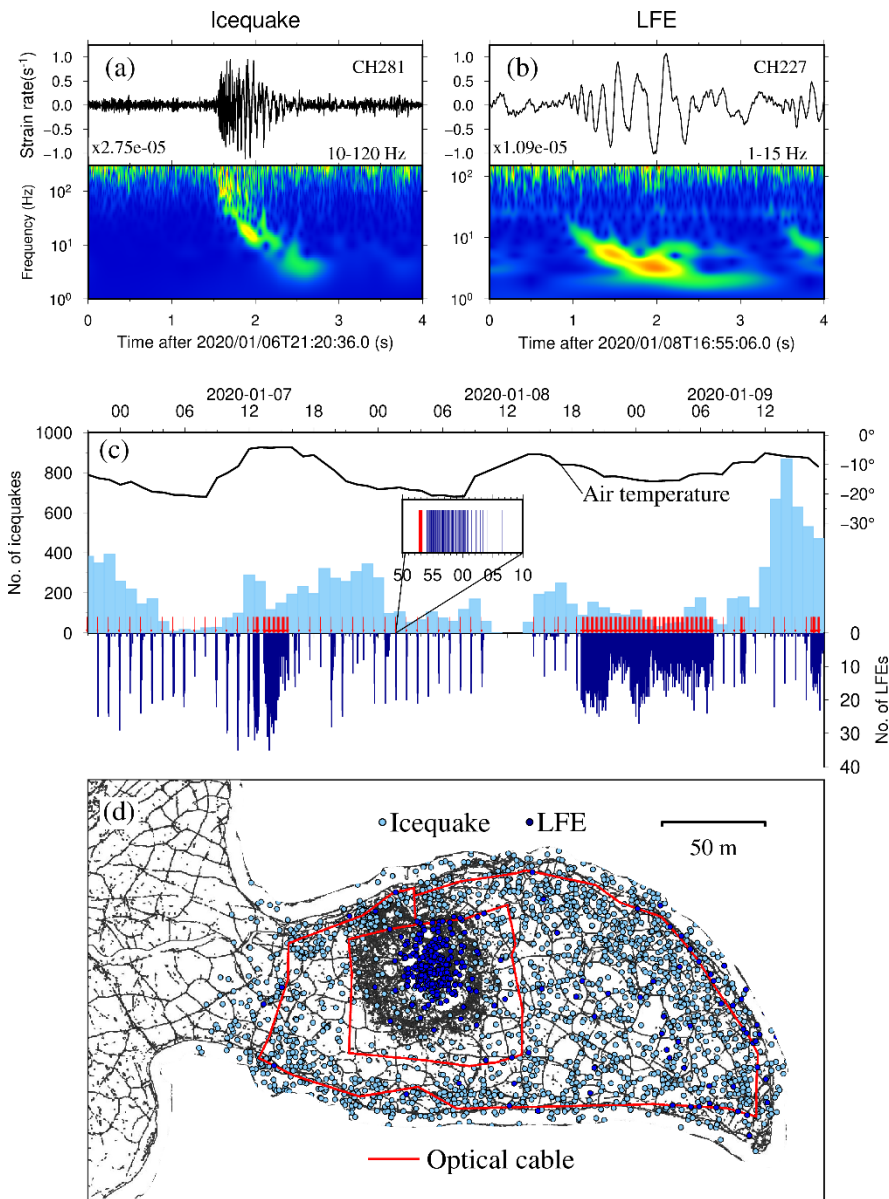
Zhu, W. and Beroza, G. C.: PhaseNet: a deep-neural-network-based seismic arrival-time picking method, *Geophysical Journal International*, 216, 261–273, <https://doi.org/10.1093/gji/ggy423>, 2019.

485



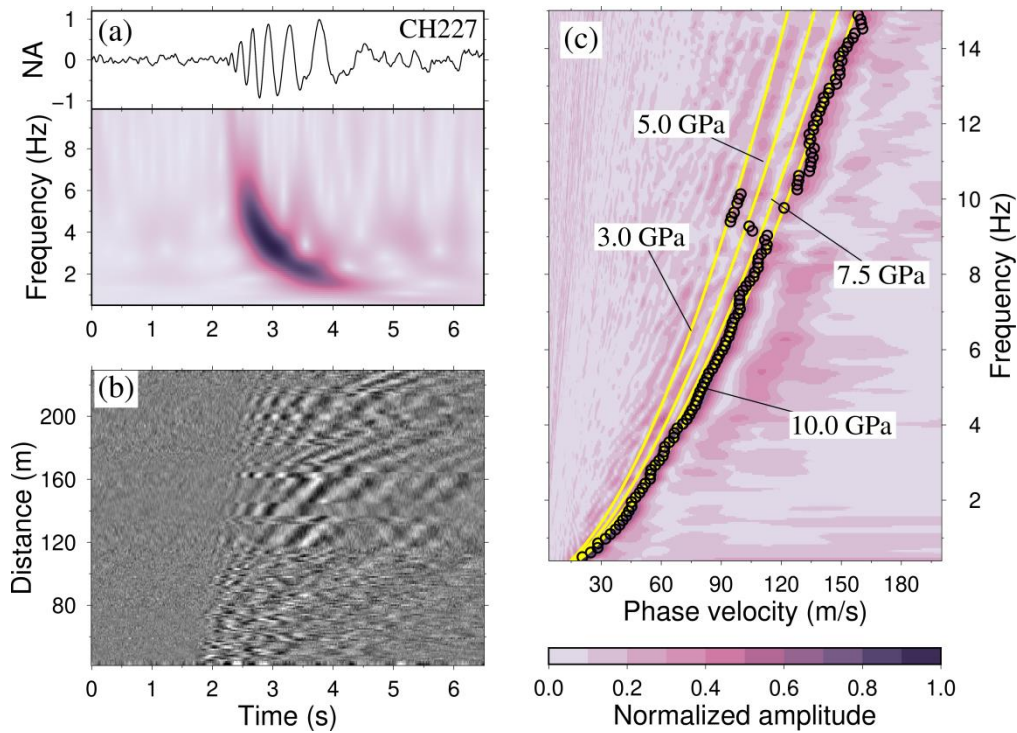
490 **Figure 1: The experimental setting.** The instrumented frozen lake is at Xiliushui Reservoir in Gansu Province, China (red rectangle in the inset). The optical fibre is marked with purple lines with channel number between 51–645 with gauge length of 10 m and a sampling rate of 1000 Hz. The airgun floating platform is at the centre of the lake. A reference broadband seismic station is marked with a triangle. Hammering points are marked with inverted triangles. The red triangle shows the one we use to measure the dispersion curve of flexural-gravity wave.





495 **Figure 2: Typical passive signal waveforms, temporal and spatial distributions.** (a) Icequake wave recorded by channel 281. The waveform is bandpass filtered in the frequency band of 10-120 Hz. (b) LFE waveform by channel 227. The waveform is bandpass filtered in the frequency band of 1-15 Hz. (c) temporal distributions for icequakes (light blue) per hour and LFEs (dark blue) per minute and the local air temperature (black curve). The temperature data is from European Centre for Medium-Range Weather Forecasts (<https://www.ecmwf.int/>). The time of AGE is marked with red arrow. The inset picture shows a window of 20 minutes with an AGE (red line) and following LFEs (black lines). The air temperature is denoted with black curve. (d) spatial distribution for icequakes (light blue) and LFEs (dark blue).

500



505 **Figure 3: Dispersion analysis of LFEs.** (a) Stacked LFE waveform and spectrogram of channel 227. The black curve is the stacked waveform with 272 LFE traces. It is bandpass filtered in the frequency band 1-15 Hz. The color denotes the normalized amplitude. (b) The record section of stacked waveform of all LFE events assuming all LFEs are originated at the AGE platform. (c) The measured phase velocity (circles) and predicted velocities (yellow curves) with different Young's modulus (3-10 GPa). The color means the dispersion spectra of stacked LFE traces in (c).